

False Data Injection Attack on Electric Vehicle-Assisted Voltage Regulation

Yuan Liu, Omid Ardakanian, Ioanis Nikolaidis, Hao Liang

Abstract—With the large scale penetration of electric vehicles (EVs) and the advent of bidirectional chargers, EV aggregators will become a major player in the voltage regulation market. This paper proposes a novel false data injection attack (FDIA) against the voltage regulation capacity estimation of EV charging stations, the process that underpins voltage regulation in distribution system. The proposed FDIA takes into account the uncertainty in EV mobility and network conditions. The attack vector with the largest expected adverse impact is the solution of a stochastic optimization problem subject to a constraint that ensures it can bypass bad data detection. We show that this attack vector can be determined by solving a sequence of convex quadratically constrained linear programs. The case studies examined in a co-simulation platform, based on two standard test feeders, reveal the vulnerability of the voltage regulation capacity estimation.

Index Terms—Cyber attacks, distribution system state estimation, electric vehicles, stochastic optimization

I. INTRODUCTION

THE notion of electric vehicle (EV) aggregators participating in the voltage regulation (VR) market has gained traction in recent years [1]. Compared to traditional VR resources, such as thermal generators, on-load tap changers (OLTC), and capacitor banks, EV battery packs offer more advantages due to their inexpensive operation, high power capacity, and fast response [2]. The EV charging station (EVCS) agent, which is a typical aggregator, can coordinate charging and discharging of all EVs that are present in the station so as to respond to VR commands issued by the distribution system operator (DSO). Since the number of plug-in EVs and their state of charge (SOC) are highly variable and uncertain, the regulation capacity provided by an EVCS can vary over time. If this capacity is underestimated, the surplus will be wasted. On the other hand, compensating the shortage in VR capacity, due to mispredictions, either increases the operation cost or negatively affects the stability of the distribution network [3]. It is therefore vital for the DSO to accurately estimate the VR capacity that can be provided by an EVCS in real time.

To facilitate the EVCS VR capacity estimation, the supervisory control and data acquisition (SCADA) system has been utilized in prior work for communications between the DSO and EVCS agents. Reliable communication is indeed required to send the collected data for further analyses, such as state estimation, and bad data detection (BDD) and correction [4]. For this reason, cyber attacks targeting the communication system are regarded as one of the major threats to the reliable

operation of power system [5]. Examples of these attacks are false data injection attacks (FDIA), denial of service and replay attacks. The FDIA could be more dangerous than other cyber attacks as it stealthier, enabling the attacker to disrupt the normal operation of the power system for a long time without being detected. Since first put forward in [6], such attacks have occurred several times, leading to long and catastrophic power outages. For example, in 2015, the attack launched against the Ukrainian power system’s SCADA caused a power outage affecting more than two million customers for six hours [7].

Prior work has investigated FDIAs against distribution system state estimation (DSSE) and proposed various methods to detect such attacks [8]–[14]. However, none of these studies accounts for the uncertainty of data communication. Since not all false data injected by the attacker is received by the system operator in a timely fashion, existing FDIA strategies may not be as stealthy as proved theoretically.

Apart from misleading the DSSE process, the FDIA can affect ancillary services that are dependent on DSSE, e.g., VR, load shifting, and frequency regulation. In [15], the authors analyze how attackers can alter multiple field measurements in a coordinated manner to disturb voltage control algorithms. A machine learning-based two-stage approach is developed subsequently for detecting such attacks. Similarly, [16] considers the impact of cyber attacks on VR in a distribution system with solar photovoltaics. An OLTC-induced FDIA against the VR process is investigated in [11]. It is shown that it can lead to a wrong OLTC tap position, causing serious under-voltage incidents. Reference [17] analyzes FDIA on battery energy storage installed in the distribution system, showing that the DSO can get completely wrong estimates of the battery energy content. Reference [18] investigates the impact of FDIA on the load redistribution process. To identify the attacker in various scenarios, a novel cooperative vulnerability factor framework is introduced in [19], where each agent can track voltage fluctuations to perform accurate detection. The impact of FDIA on remedial action schemes and the extent of failure propagation have been studied in [20]. In [21], the authors propose a Luenberger observer and an artificial neural network-based approach to detect attacks against the load frequency control system.

Despite the vast literature in this area, there are still several challenges that are not fully addressed. First, most related work relies on DC power flow, which is known to be inaccurate in certain distribution networks. Second, an idealized communication model is usually adopted, ignoring the impact of packet losses and delays on FDIA. Third, the related work does not investigate the vulnerability of the VR process to an FDIA when the DSO does not receive the attack vector completely.

This paper aims to address the gap that is identified above. Specifically, we propose a novel approach for attack vector

This research was supported by funding from the Canada First Research Excellence Fund as part of the University of Alberta’s Future Energy Systems research initiative.

Y. Liu (email: yuan17@ualberta.ca) and H. Liang (email: hao2@ualberta.ca) are with the Department of Electrical and Computer Engineering, University of Alberta, Canada. O. Ardakanian (email: oardakan@ualberta.ca) and I. Nikolaidis (email: nikolaidis@ualberta.ca) are with the Department of Computing Science, University of Alberta, Canada.

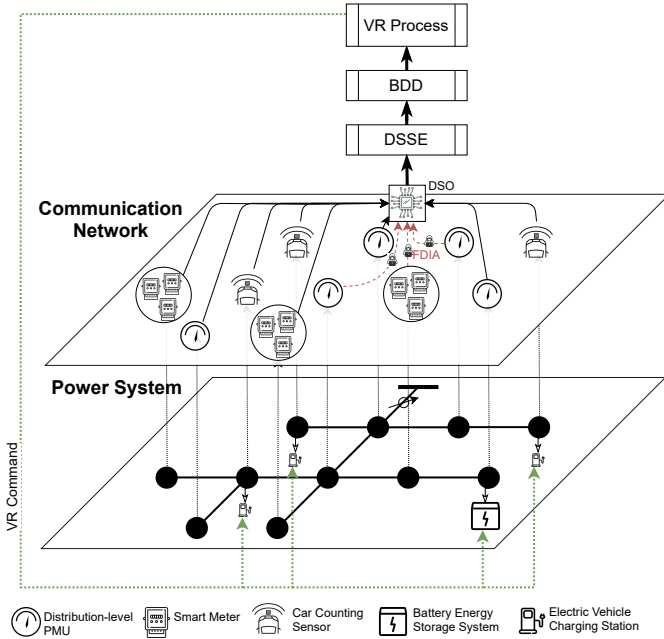


Fig. 1: Illustration of FDIA against the VR process in a distribution system with EVCS and traditional VR resources, e.g., BESS. Red dashed lines show where the attacker injects false data.

construction using a stochastic communication model. Our approach relies on AC power flow and a probabilistic model that captures the uncertainty of the EVCS up-regulation and down-regulation capacities. We investigate the vulnerability of DSSE and BDD mechanism, underpinning the VR process, to the proposed FDIA. The contribution of this paper is threefold:

- We develop a realistic VR model by extending DSSE and BDD with AC power flow analysis, and considering the locations of charging stations in the distribution network.
- We propose an FDIA vector construction method that relies on a stochastic communication model. The optimal attack vector, which is the solution of a stochastic optimization problem, can be found by comparing the solutions of a sequence of convex optimization problems.
- Through co-simulation, we expose the vulnerability of EVCS-assisted VR to the proposed FDIA. Our case studies, involving IEEE 33-bus and 123-bus test feeders, suggest that the proposed FDIA is potentially more harmful than the traditional FDIA which relied on an idealized communication model. This calls for the development of advanced BDD mechanisms that factor in varying network conditions, a promising direction for future work.

The remainder of this paper is organized as follows. Section II introduces the models, DSSE, and BDD process. Section III presents the proposed attack vector construction method under idealized and stochastic communication models. Section IV describes the case studies and the results obtained via co-simulation. Section V concludes the paper and presents avenues for future work.

II. SYSTEM MODEL

Fig. 1 shows a power distribution network with various VR resources, such as battery energy storage systems (BESS), distributed generation units, and EV charging stations. The distribution network is instrumented with a small number of

distribution-level PMUs and numerous smart meters that are installed at customers' premises. These sensors can be used to monitor the system state. We assume sensor measurements are time-synchronized and sent at regular intervals (of length Δt) to the DSO control centre located at the substation through a communication network. Similarly, the number of EVs parked at each EVCS is periodically sent to this control centre.

Due to random packet losses that could occur in the communication network and sparse deployment of distribution-level PMUs, the DSO may have to use historical data to obtain pseudo measurements. Together with real-time measurements, these pseudo measurements are used in the DSSE, the output of which is sent through the BDD process to determine if it can be trusted. If the estimated state passes the BDD process successfully, it will be utilized to issue control signals to the VR resources. Otherwise, the state estimate obtained by using pseudo measurements is utilized to issue control signals.

Given the reliance of DSSE on real-time measurements, an attacker can target PMUs and EV counters for false data injection to deceive the DSO into overestimating the VR capacity. Yet, to minimize the risk of being detected, it should account for the stochasticity of data transmission that could result in pseudo measurements being used in lieu of real-time sensor measurements when they are not received by the time DSSE is run. We assume that the attacker has knowledge of the distribution system model, and unrestricted access to PMU measurements, EV counts, and the corresponding historical data that can be used to obtain pseudo measurements. Furthermore, we make the following assumptions in this work:

- 1) The DSO performs DSSE and sends VR commands at regular intervals;
- 2) EVs take precedence over other VR resources in the VR process due to their responsiveness and low cost operation. Hence, they are always used first;
- 3) Every EV that is plugged into a charger in an EVCS is willing to act as a VR resource as long as its charging demand is guaranteed to be satisfied before departure¹;
- 4) There is enough parking stalls in each EVCS so that all EVs are admitted upon arrival. But there might be a cap on the number of active chargers or the power that can be drawn simultaneously². The remaining parking stalls are occupied by EVs that are waiting for service;
- 5) A car counter sensor is installed at each EVCS. This sensor tracks the total number of EVs that are idle or being charged, without error.

We now present the models adopted for voltage regulation, EVCS load, stochastic communication, BDD, and power flow.

A. Voltage Regulation in Distribution System

We consider a balanced three-phase distribution network with the set of nodes denoted $\mathbf{N} = \{1, \dots, N\}$. We denote the voltage magnitude, phase angle, active power injection, and reactive power injection of node n at time t by $\mathbf{V}_t = \{v_{n,t}\}$,

¹A fraction of the revenue generated from the EVCS participation in VR can be distributed among EVs to incentivize them to allow the EVCS to use their battery for voltage regulation. That said, the design of this mechanism is outside the scope of this paper.

²The upper limit is imposed by the utility to avoid transformer overloading.

$\theta_t = \{\theta_{n,t}\}$, $\mathbf{P}_t = \{p_{n,t}\}$, $\mathbf{Q}_t = \{q_{n,t}\}$, respectively. Suppose there is a subset of nodes $\mathbf{E} = \{1, \dots, E\} \subseteq \mathbf{N}$ where the connected load is an EVCS. An EVCS at node $e \in \mathbf{E}$ can provide up-regulation capacity of $p_{e,t}^U$ and down-regulation capacity of $p_{e,t}^D$ at time t . We use the VR process described in [22], [23]. Specifically, the goal is to keep the average nodal voltage magnitude within an acceptable range $[v^{\min}, v^{\max}]$ around the reference voltage v^R and preferably close to v^R . Hence, the VR objective function is formulated as the squared deviation from the reference voltage averaged over all nodes:

$$\min_{\{p'_{e,t} | e \in \mathbf{E}\}} \frac{1}{N} \sum_{n=2}^N (v^R - v_{n,t})^2 \quad (1a)$$

$$s.t. \quad p_{e,t} - p'_{e,t} \leq p_{e,t}^D, e \in \mathbf{E} \quad (1b)$$

$$p'_{e,t} - p_{e,t} \leq p_{e,t}^U, e \in \mathbf{E} \quad (1c)$$

$$v^{\min} \leq v_{n,t} \leq v^{\max}, n \in \mathbf{N}, \quad (1d)$$

where $p'_{e,t}$ is the active power contribution of EVCS e when participating in VR. Given the distribution network structure, it is possible that charging stations that offer the same up- and down-regulation capacities but are connected to different nodes, contribute differently in the VR process. Thus, we need to quantify the EVCS VR capacity based on its impact on the voltage magnitude of node n given by

$$\Delta v(n) = g_n^V(\mathbf{P}_t, \mathbf{Q}_t, \mathbf{P}_t^D, \mathbf{P}_t^U), \quad (2)$$

where $\mathbf{P}_t^D = \{p_{1,t}^D, \dots, p_{E,t}^D\}$, $\mathbf{P}_t^U = \{p_{1,t}^U, \dots, p_{E,t}^U\}$ are the sets of up- and down-regulation capacities of all EVCSs, $g^V(\cdot)$ is a function representing the maximum difference in the voltage magnitude of node n that could be caused when the full VR capacity of the EVCS is utilized. This function can be derived from power flow equations. The total VR capacity of the distribution network can be defined as

$$\Delta v = \sum_{n \in \mathcal{E}} \Delta v(n), \quad (3)$$

where $\mathcal{E} \subseteq \mathbf{N}$ is a subset of nodes in the distribution network that suffer from voltage limit violation problems. These nodes are typically at the end of distribution feeders.

B. Stochastic Process for Characterizing the Number of EVs

Suppose EVCS e has L_e charging points and EVs arrive at this charging station following a Poisson process with rate λ_e . Hence, the probability of having one arrival in a short time slot of length τ is $q_a = \lambda_e \tau + o(\tau)$ and the probability of no arrival in that time slot is $q'_a = 1 - \lambda_e \tau + o(\tau)$. Suppose the EV charging times are independent and identically distributed exponential random variables with mean $1/\mu_e$. Hence, the probability of having one departure from a specific active charger (i.e., charge service completion) in a short time slot is $q_d = \mu_e \tau + o(\tau)$, and the probability of no departure from that charger in that time slot is $q'_d = 1 - \mu_e \tau + o(\tau)$. Note that $o(\tau)$ terms are negligible compared to τ when τ is sufficiently small; thus, they are ignored (infinitesimal asymptotics).

Let us denote the total number of charging and idling EVs in EVCS e by $c_{e,t} \leq L_e$. Hence, $\mathbf{C}_t = \{c_{1,t}, \dots, c_{e,t}, \dots, c_{E,t}\}$ is the set that contains the number of EVs that are in one of

the E stations at time t . Assuming that there are $c_{e,t} = n$ EVs in EVCS e at t , we can derive the probability of having $n+i$ EVs in this EVCS at $t+1$ as follows:

$$P(c_{e,t+1} = n+i | c_{e,t} = n) = \begin{cases} q_a q_d^n & i = 1 \\ q'_a q_d^n & i = -n \\ \binom{n}{i} q'_a q_d^{-i} q_d^{n+i} + \binom{n}{i+1} q_a q_d^{1-i} q_d^{n+i-1} & -n < i < 1 \\ 0 & \text{otherwise} \end{cases} \quad (4)$$

where $\binom{n}{i}$ is a binomial coefficient. The DSO uses this probabilistic model to compute the most probable number of EVs in the EVCS, treated as the pseudo measurement, when it does not receive the real-time measurement of the respective EV counter by the time it performs DSSE.

We now estimate the number of time slots in which an EV can participate in VR. Suppose an EV arrives at the EVCS at t with the initial SOC s^I , battery size e^B , charge (and discharge) power p^C , target SOC s^T and expected parking time t^P . The expected charging time for this EV would be:

$$t^C = \begin{cases} \frac{(s^T - s^I)e^B}{p^C}, & s^I < s^T \\ 0, & s^I \geq s^T \end{cases} \quad (5)$$

Naturally, EV owners seek to charge their car to the target SOC before departure. Once the current SOC reaches the target SOC, the EVCS aggregator will be able to charge or discharge the EV battery to provide up- or down-regulation. In this case, the corresponding charge/discharge power contributes to the VR capacity of the EVCS. However, to compensate for the energy withdrawn from the EV battery in the VR process, the battery must be recharged to the target SOC before the EV departure. Thus, the time slots available for providing VR capacity are as follows.

$$t^V = \begin{cases} \lfloor (t^P - t^C)/2 \rfloor, & t^C < t^P \\ 0, & t^C \geq t^P \end{cases} \quad (6)$$

where $\lfloor \cdot \rfloor$ is the floor function. Note that if the time required to satisfy the energy demand of an EV is longer than its parking time, the EV will be charged until departure without providing any VR capacity. Since the expected charging time and parking time are known in advance, the EVCS aggregator can flexibly control the EV charging process. In other words, the t^V time slots can be utilized to provide the VR capacity when appropriate³.

The EVs that arrive at the EVCS can have various initial SOC, battery sizes, and parking times. We denote the probability density function for the initial SOC and parking time by $f_S(\cdot)$ and $f_P(\cdot)$ respectively. Similarly, we denote the probability mass function for the battery size and maximum charge/discharge power by $\varrho_B(\cdot)$ and $\varrho_C(\cdot)$, respectively.

C. Stochastic Model for Data Transmission

Suppose U distribution-level PMUs are installed at nodes $\mathbf{U} = \{1, \dots, U\}$ to monitor the voltage magnitude and phase

³It might be the case that some EV owners only allow their battery to be used for VR after their original energy demand is supplied. In that case, the time slots available to provide the VR capacity are fixed. Even in that case, the method proposed in this work is applicable as discussed in Section III-B.

angle. They send their measurements to the DSO at the end of each time slot, which are then used to carry out DSSE t time slots after the measurements are taken. The measurement packets that are not received by the control centre after t time slots are deemed lost, and the respective pseudo measurements will be utilized in the DSSE process.

Following the Gilbert–Elliott model, we model changes in data transmission using a two-state Markov chain [24]. In this chain, the good state (G) represents successful transmission, and the bad state (B) represents unsuccessful transmission (i.e., the packet is not received after t time slots). The transition probability matrix of this chain is

$$\begin{bmatrix} 1 - \kappa^{GB} & \kappa^{GB} \\ \kappa^{BG} & 1 - \kappa^{BG} \end{bmatrix},$$

where κ^{GB} is the probability of going from a good state to a bad state and κ^{BG} is the probability of going from a bad state to a good state. Thus, the stationary distribution of this Markov chain can be written as

$$\pi(G) = \frac{\kappa^{BG}}{\kappa^{GD} + \kappa^{BG}}, \quad \pi(B) = \frac{\kappa^{GB}}{\kappa^{GD} + \kappa^{BG}}, \quad (7)$$

where $\pi(G)$ is the steady-state probability of being in a good state and $\pi(B)$ is the steady-state probability of being in a bad state. This implies that in the steady state, real-time PMU measurements are used in the DSSE process with probability $\pi(G)$ and pseudo measurements are used with probability $\pi(B) = 1 - \pi(G)$.

Based on the Gilbert–Elliott model, we can model the communication between sensors and the DSO control centre as independent Markov processes. We use binary vectors $\phi^U = [\phi_1^U, \dots, \phi_U^U]$ and $\phi^E = [\phi_1^E, \dots, \phi_E^E]$ to collect the outcomes of data transmission in time slot t for all PMUs and EV counters. We use $\phi = [\phi^U, \phi^E]^\top$ to compactly represent both vectors, the size of which is $U + E$.

D. DSSE with BDD

The DSSE concerns estimating the distribution system operating conditions given the measurement of a set of state variables [25], e.g., nodal voltage magnitude and phase angle, real and reactive power injection at nodes, and real and reactive power flow in branches. The relation between the measurement z and the system state x is given by:

$$z = h(x) + \varepsilon, \quad (8)$$

where $h(\cdot)$ is a nonlinear function that relates the measurement to the system state, and ε is the measurement noise with covariance matrix \mathbf{R} . We note that $h(\cdot)$ depends on the distribution system structure and line parameters. Given z , $h(\cdot)$, and \mathbf{R} , the system state x can be estimated by solving a weighted least squares (WLS) problem [26]:

$$\hat{x} = \arg \min_x [z - h(x)]^\top \mathbf{W} [z - h(x)], \quad (9)$$

where $\mathbf{W} = \text{diag}\{\mathbf{R}^{-1}\}$ and $[\cdot]^\top$ denotes matrix transposition. This optimization problem can be solved via an iterative approximation method, such as the Newton-Raphson method. However, nonlinearity of $h(\cdot)$ increases the computation overhead to a great extent. More importantly, its convergence

cannot be guaranteed. Thus, this optimization problem is often simplified by linearizing the power flow equations. Consequently, $h(\cdot)$ is given by

$$h(x) = \mathbf{H}x, \quad (10)$$

where \mathbf{H} is the measurement matrix obtained from the linearized power flow equations (we can also use the Jacobian matrix). In this case, the estimate can be derived as follows:

$$\begin{aligned} \hat{x} &= \arg \min_x [z - \mathbf{H}x]^\top \mathbf{W} [z - \mathbf{H}x] \\ &= (\mathbf{H}^\top \mathbf{W} \mathbf{H})^{-1} \mathbf{H}^\top \mathbf{W} z. \end{aligned} \quad (11)$$

Considering the measurement noise of sensors and the possibility that measurements are modified by an attacker, DSOs typically employ a residual-based BDD mechanism to protect the DSSE process. In this context, the residual can be defined as the difference between the actual measurement z and the measurement that corresponds to the estimated system state, i.e., $\hat{z} = \mathbf{H}\hat{x}$. Then, by comparing the Euclidean norm of the residual $r = z - \hat{z}$ against a threshold ϵ , false data or erroneous measurement can be detected (if $\|r\|_2 > \epsilon$). Otherwise, the estimated system state \hat{x} can be trusted. The value of ϵ is typically determined by a hypothesis test $P(\|r\|_2 > \epsilon) < \tau$, where τ is the significance level.

In the VR process, the real-time system state is defined as $x = [\mathbf{P}_t, \mathbf{Q}_t, \mathbf{P}_t^D, \mathbf{P}_t^U]^\top$ and the measurement vector is denoted by $z = [\mathbf{V}_t, \boldsymbol{\theta}_t, \mathbf{C}_t]^\top$. The vectors \mathbf{V}_t , $\boldsymbol{\theta}_t$, and \mathbf{C}_t collect real-time measurements and pseudo measurements according to the communication result.

E. Linear Power Flow Analysis

We use a linear power flow analysis method to solve the DSSE problem more effectively. Let us denote the resistance and reactance between node n and k by r_{nk} and x_{nk} , respectively. According to [27], we can approximate $\Delta\theta_{ik} \approx 0$ and $v_i \approx 1$ p.u. This allows us to linearize the power flow equations and write them in matrix form:

$$\begin{bmatrix} \boldsymbol{\theta}' \\ \mathbf{v}' \end{bmatrix} = \begin{bmatrix} \mathbf{M}^{2'} & \mathbf{M}^{1'} \\ -\mathbf{M}^{1'} & \mathbf{M}^{2'} \end{bmatrix}^{-1} \left(\begin{bmatrix} \mathbf{p}' \\ \mathbf{q}' \end{bmatrix} - \begin{bmatrix} \mathbf{m}^{2c} \\ -\mathbf{m}^{1c} \end{bmatrix} \theta_1 - \begin{bmatrix} \mathbf{m}^{1c} \\ \mathbf{m}^{2c} \end{bmatrix} v_1 \right), \quad (12)$$

where $\boldsymbol{\theta}'$, \mathbf{v}' , \mathbf{p}' and \mathbf{q}' are respectively the voltage phase angle, voltage magnitude, active power, and reactive power vectors of all the buses, except the slack bus. Here \mathbf{m}^{1c} and \mathbf{m}^{2c} are the first columns of \mathbf{M}^1 and \mathbf{M}^2 respectively, while $\mathbf{M}^{1'}$ and $\mathbf{M}^{2'}$ are respectively the sub-matrices of \mathbf{M}^1 and \mathbf{M}^2 when we ignore the first column and the first row. Note that \mathbf{M}^1 and \mathbf{M}^2 are constant matrices obtained from the admittance matrix with their elements given by

$$M_{nk}^1 = \frac{r_{nk}}{r_{nk}^2 + x_{nk}^2}, \quad n \neq k, \quad (13a)$$

$$M_{nk}^2 = \frac{x_{nk}}{r_{nk}^2 + x_{nk}^2}, \quad n \neq k, \quad (13b)$$

$$M_{nk}^1 = \sum_{k=\{1, \dots, N\} - \{n\}} \frac{r_{nk}}{r_{nk}^2 + x_{nk}^2}, \quad (13c)$$

$$M_{nk}^2 = \sum_{k=\{1, \dots, N\} - \{n\}} \frac{x_{nk}}{r_{nk}^2 + x_{nk}^2}. \quad (13d)$$

Based on (12), the voltage magnitude and phase angle can be written as a linear function of \mathbf{P} and \mathbf{Q} :

$$v_n = \sum_{k=2}^N M_{nk}^2 p_k + \sum_{k=2}^N M_{nk}^1 q_k + m_n^V, \quad (14)$$

$$\theta_n = \sum_{k=2}^N M_{nk}^2 p_k + \sum_{k=2}^N M_{nk}^1 q_k + m_n^\theta, \quad (15)$$

where m_n^V and m_n^θ are a constant value given by

$$\begin{aligned} & [m_2^V, \dots, m_N^V, m_2^\theta, \dots, m_N^\theta]^\top \\ &= - \begin{bmatrix} \mathbf{M}^{2'} & \mathbf{M}^{1'} \\ -\mathbf{M}^{1'} & \mathbf{M}^{2'} \end{bmatrix}^{-1} \left(\begin{bmatrix} \mathbf{m}^{2c} \\ -\mathbf{m}^{1c} \end{bmatrix} \theta_1 + \begin{bmatrix} \mathbf{m}^{1c} \\ \mathbf{m}^{2c} \end{bmatrix} v_1 \right). \end{aligned} \quad (16)$$

III. STOCHASTIC FDIA ON VOLTAGE REGULATION

In the previous section, the system state has been augmented with the variables that are necessary for VR, namely up-regulation capacity, down-regulation capacity, and EV counts. Given this new definition, a modified DSSE framework would be needed for the DSO to estimate the system states. In this section, we first develop an optimization-based method for FDIA vector construction assuming an idealized communication model. We then present a new framework for DSSE that takes the VR variables into account. This framework is utilized to formulate an optimization problem for FDIA vector construction under a stochastic communication model.

A. FDIA against VR under Idealized Communication Model

Under the idealized communication model, sensor data is guaranteed to be received before running DSSE, hence pseudo measurements are not used at all. In this case, the attacker's objective to perturb measurements such that the adverse impact on the distribution network is maximized. We define the impact of an FDIA by comparing the VR capacity before and after this attack:

$$\psi_\phi(\boldsymbol{\alpha}) = \Delta v_\phi^A - \Delta v_\phi, \quad (17)$$

where ϕ is a 1-vector here because all packets must be received on time under the idealized model, Δv_ϕ is defined in (3), and Δv_ϕ^A is the same quantity under FDIA. The best FDIA vector can be determined by solving the optimization problem below:

$$\max_{\boldsymbol{\alpha}} \psi_\phi(\boldsymbol{\alpha}) \quad (18a)$$

$$s.t. \quad \mathbf{z}^A = \mathbf{z} + \boldsymbol{\alpha} \quad (18b)$$

$$\hat{\mathbf{x}}^A = \boldsymbol{\Omega} \mathbf{z}^A \quad (18c)$$

$$\mathbf{r}^A = \mathbf{z}^A - \mathbf{H} \hat{\mathbf{x}}^A \quad (18d)$$

$$\|\mathbf{r}^A\|_2 \leq \epsilon \quad (18e)$$

Here $\boldsymbol{\alpha}^U = [\alpha_1^U, \dots, \alpha_V^U]$ and $\boldsymbol{\alpha}^E = [\alpha_1^E, \dots, \alpha_E^E]$ are the attack vectors concerning PMUs and EV counters (in charging stations); $\boldsymbol{\alpha} = [\boldsymbol{\alpha}^U, \boldsymbol{\alpha}^E]^\top$ is the combined attack vector; \mathbf{z}^A represents the modified measurements; $\boldsymbol{\Omega} = (\mathbf{H}^\top \mathbf{W} \mathbf{H})^{-1} \mathbf{H}^\top \mathbf{W}$ is the estimation matrix obtained from (11). Note that the objective function is linear because we have linearized the power flow equations and estimation function.

B. Modified DSSE with VR Variables

Conventionally in DSSE, $h(\cdot)$ is obtained through power flow analysis to calculate the voltage magnitude and phase angle measurements given the real and reactive loads. But when the VR variables are added to the state, a new function must be derived to estimate the VR capacity according to the extended system state, i.e., $\mathbf{z} = [\mathbf{V}_t, \boldsymbol{\theta}_t, \mathbf{C}_t]^\top$. In this section, we first try to obtain the inverse of $h(\cdot)$ which relates the EV counts to VR capacity. Knowing the inverse function, we derive $h(\cdot)$ at the end of this section.

Suppose one EV is parked at stall ℓ in EVCS e in time slot t . This EV can be represented using a vector $[t_0, t^P, t^C, s^I, p^C, b^E]$, where $t_0 \leq t$ is the arrival time slot and we have a constraint that $t - t_0 \leq t^P$. Given $p_{e,t}$, which denotes the active load of EVCS e obtained from the power flow analysis, we can estimate the expected number of charging EVs in this station at time t as follows

$$c_{e,t}^C = p_{e,t} / \sum_{\forall p^C} p^C \cdot \varrho_C(p^C) \quad (19)$$

Accordingly, the expected number of idling EVs in this station can be calculated from $c_{e,t}^I = c_{e,t} - c_{e,t}^C$.

We consider two charging modes: *strict* and *flexible*. The distinction between these two modes is whether or not an EV can participate in VR before its initial charging demand is satisfied. More specifically, a charging EV in the strict charging mode cannot provide up- or down-regulation capacity. But, for an idling EV in the strict charging mode, the up- and down-regulation capacities are given by

$$p_{e,\ell,t}^D = \begin{cases} p^C, & s^I + p^C \Delta t \leq s^T \\ 0, & \text{otherwise} \end{cases}, \quad (20)$$

$$p_{e,\ell,t}^U = \begin{cases} p^C, & t^V > 0 \\ 0, & \text{otherwise} \end{cases}. \quad (21)$$

Turning our attention to the flexible charging mode, the down-regulation capacity of a charging EV is zero. If a charging EV has abundant parking time, it can stop charging and immediately discharge its battery to provide the up-regulation capacity of $2 p^C$:

$$p_{e,\ell,t}^U = \begin{cases} 2 p^C, & t^P > t^C \\ 0, & \text{otherwise} \end{cases}. \quad (22)$$

The up- and down-regulation capacities of an idling EV are exactly the same as a charging EV (see Eq. (20) and (21)).

Given the probability density and mass functions, i.e., $f_S(\cdot)$, $\varrho_B(\cdot)$, $\varrho_C(\cdot)$, and $f_P(\cdot)$, our goal is to estimate the VR capacity of an arbitrary EV in an EVCS. To this end, we need to derive the probability distribution of t^C based on the probability distribution of b^E , p^C , and s^I [28]:

$$\begin{aligned} & f(t^C) \\ &= \begin{cases} 0, & t^C \notin (0, t^P) \\ 1 - \int_0^{t^C} f_P(t^P) dt^P, & t^C = t^P \\ \sum_{b^E} \varrho_B(b^E) \sum_{p^C} \varrho_C(p^C) \int_0^{s^T} f_S(s^I) \delta(C^T) ds^I, & \text{otherwise} \end{cases} \end{aligned}$$

where $\delta(\cdot)$ is the Dirac delta function and $C^T = t^C - \frac{(s^T - s^I)b^E}{p^C}$. The probability distribution of the flexible VR time can be calculated as follows:

$$f(t^V) = \int_0^\infty f(t^P) \int_0^{t^P} f(t^C) \delta(C^V) dt^C dt^P,$$

where $C^V = t^V - \lfloor (t^P - t^C)/2 \rfloor$. Accordingly, the probability that an idling/charging EV has some available VR time slot is

$$P(t^V > 0, t^C < t - t_0) = \sum_{t^V} \int_0^\infty P(t^P) \int_0^{t-t_0} f(t^C) \delta(C^V) dt^C dt^P, \quad (23)$$

$$P(t^V > 0, t^P > t^C \geq t - t_0) = \sum_{t^V} \int_0^\infty P(t^P) \int_{t-t_0}^{t^P} f(t^C) \delta(C^V) dt^C dt^P. \quad (24)$$

Given the expected EV charging time t^C and arrival time t_0 , the probability that it is idling at time t is $P(t^C < t - t_0)$ which is given by

$$P(t^C < t - t_0) = \int_0^{t-t_0} f(t^C) dt^C, \quad (25)$$

and the probability that it is charging is $P(t^P > t^C \geq t - t_0)$ which is given by

$$P(t^P > t^C \geq t - t_0) = \int_{t-t_0}^{t^P} f(t^C) dt^C. \quad (26)$$

Observe that $t^C < t - t_0$ and $s^I + p^C \Delta t \leq s^T$ are not independent events. We derive the conditional probability $P(t^C | s^I, p^C)$ as follows:

$$P(t^C | s^I, p^C) = \begin{cases} \sum_{b^E} P^E(b^E) \mathbf{I}_{C^T=0}(b^E), & 0 < t^C < t^P \\ 1 - \int_0^{t^P} f(t^C) dt^C, & t^C = t^P \\ 0, & \text{otherwise} \end{cases} \quad (27)$$

where $\mathbf{I}_{C^T=0}$ is the indicator function of set $\{b | C^T = 0\}$, i.e., it is equal to 1 when b^E satisfies the equation $C^T = 0$, and is 0 otherwise. We can write:

$$P(t^C < t - t_0, s^I + p^C \Delta t \leq s^T) = \int_0^{t-t_0} P(t^C | s^I, p^C) \sum_{\forall p^C} P(p^C) \int_0^{s^T} s^I \delta(C^T) ds^I dt^C. \quad (28)$$

Based on the analysis above, the expected VR capacity of an EV in the strict charging mode is given by

$$\bar{p}_{e,\ell,t}^{ID} = p^C \frac{P(t^C < t - t_0, s^I + p^C \Delta t \leq s^T)}{P(t^C < t - t_0)}, \quad (29)$$

$$\bar{p}_{e,\ell,t}^{CD} = 0, \quad (30)$$

$$\bar{p}_{e,\ell,t}^{IU} = p^C \frac{P(t^V > 0, t^C < t - t_0)}{P(t^C < t - t_0)}, \quad (31)$$

$$\bar{p}_{e,\ell,t}^{CU} = 0, \quad (32)$$

and the expected VR capacity of an EV in the flexible charging

mode is given by

$$\bar{p}_{e,\ell,t}^{ID} = p^C \frac{P(t^C < t - t_0, s^I + p^C \Delta t \leq s^T)}{P(t^C < t - t_0)}, \quad (33)$$

$$\bar{p}_{e,\ell,t}^{CD} = 0, \quad (34)$$

$$\bar{p}_{e,\ell,t}^{IU} = p^C \frac{P(t^V > 0, t^C < t - t_0)}{P(t^C < t - t_0)}, \quad (35)$$

$$\bar{p}_{e,\ell,t}^{CU} = p^C \frac{P(t^V > 0, t^C < t - t_0)}{P(t^C < t - t_0)} + 2p^C \frac{P(t^V > 0, t^P > t^C \geq t - t_0)}{P(t^C < t - t_0)}. \quad (36)$$

where $\bar{p}_{e,\ell,t}^{ID}$ and $\bar{p}_{e,\ell,t}^{IU}$ represent the down- and up-regulation capacities of an idling EV, and $\bar{p}_{e,\ell,t}^{CD}$ and $\bar{p}_{e,\ell,t}^{CU}$ represent the same quantities for a charging EV. Putting it all together, the total VR capacity of an EVCS can be estimated using a linear function of the total number of charging and idling EVs in that station:

$$\bar{p}_{e,t}^D = \bar{p}_{e,\ell,t}^{ID} c_{(e,t)}^I + \bar{p}_{e,\ell,t}^{CD} c_{(e,t)}^C, \quad (37)$$

$$\bar{p}_{e,t}^U = \bar{p}_{e,\ell,t}^{IU} c_{(e,t)}^I + \bar{p}_{e,\ell,t}^{CU} c_{(e,t)}^C. \quad (38)$$

Recall that the voltage magnitude and phase angle of each node can also be calculated from (14) and (15), which are linear. Thus, the inverse of $h(\cdot)$ is a linear function of measurement z , and can be written in matrix form. This allows us to write $h(\cdot)$ in matrix form too.

C. FDIA against VR under Stochastic Communication Model

Due to stochastic packet drops in the communication network, the measurement sent by PMUs may not be received by the DSO when it attempts to run DSSE, causing the respective pseudo measurements to be used in the process instead. Let us denote the measurement vector utilized by the DSO in DSSE by $z^R = \phi z + (1 - \phi) z^P$, where $\mathbf{1}$ is the 1-vector, ϕ is a binary vector that indicates sensor measurements that are successfully received by the DSO, and z^P is the pseudo measurement vector. Similarly, we define $z^{AR} = \phi z^A + (1 - \phi) z^P$ to be the measurement utilized in DSSE when FDIA is performed. We write the joint probability distribution of the communication results as

$$P(\phi) = \prod_{\{i|\phi_i=1\}} \pi(G) \prod_{\{j|\phi_j=0\}} \pi(B), \quad (39)$$

and the probability of receiving measurement vector z^R as

$$P(z^R) = \sum_{\{\phi|z^R=\phi z+(1-\phi)z^P\}} P(\phi). \quad (40)$$

Hence, the probability of obtaining a state estimate \hat{x} from DSSE given the measurement z^R is

$$P(\hat{x}) = \sum_{\{z^R|\Omega z^R=\hat{x}\}} P(z^R), \quad (41)$$

and the corresponding residual is

$$r = z^R - \hat{z} = z^R - \mathbf{H}\Omega z^R. \quad (42)$$

The probability distribution over the residuals can be calculated as follows

$$P(\mathbf{r}) = \sum_{\{\mathbf{z}^R | \mathbf{z}^R - \mathbf{H}\Omega(\mathbf{z}^R) = \mathbf{r}\}} P(\mathbf{z}^R). \quad (43)$$

Recall that the total VR capacity can be calculated in terms of voltage magnitude differences according to (3). From (14) and (15), the voltage magnitude difference can be calculated as a linear function of node active and reactive loads along with up- and down-regulation capacities of every EVCS. The up- and down-regulation capacities themselves are linear functions of EV counts as shown in (37) and (38). Thus, the Δv term in (3) is a linear function of the DSSE result, $\hat{\mathbf{x}}$, and can be written as

$$\Delta v = \mathcal{V}\Omega\mathbf{z}, \quad (44)$$

where \mathcal{V} can be derived from (3), (14), (15), (37), and (38). This yields a probability distribution over the VR capacity

$$P(\Delta v) = \sum_{\{\hat{\mathbf{x}} | \hat{\mathbf{x}} = \Delta v\}} P(\hat{\mathbf{x}}). \quad (45)$$

Following the same approach, we can obtain the DSSE result given an attack vector α . We add A to the subscript to mark the variables related to FDIA.

Given the derivations above, we formulate an optimization problem for the FDIA vector construction under the stochastic communication model:

$$\max_{\alpha} \Psi(\alpha) \quad (46a)$$

$$s.t. \quad \Psi(\alpha) = \sum_{\{\phi\}} \eta_{\phi}(\alpha) P(\Delta v_{\phi}^A) \psi_{\phi}(\alpha) \quad (46b)$$

$$\hat{\mathbf{x}}_{\phi}^A = \Omega \mathbf{z}_{\phi}^{AR} \quad \forall \phi \quad (46c)$$

$$\Delta v_{\phi}^A = \mathcal{V} \hat{\mathbf{x}}_{\phi}^A \quad \forall \phi \quad (46d)$$

$$\mathbf{r}_{\phi}^A = \mathbf{z}_{\phi}^{AR} - \mathbf{H} \hat{\mathbf{x}}_{\phi}^A \quad \forall \phi \quad (46e)$$

$$\eta_{\phi} = \begin{cases} 1, & \|\mathbf{r}_{\phi}^A\|_2 \leq \epsilon \\ 0, & \text{otherwise} \end{cases} \quad \forall \phi \quad (46f)$$

where $\eta_{\phi}(\alpha)$ is the BDD result associated with attack vector α and communication result ϕ . The optimal point of this problem is the attack vector that has the largest expected adverse impact on the VR process. Notice that, for a specific communication result ϕ , $P(\Delta v_{\phi}^A)$ is constant and $\psi_{\phi}(\alpha)$ is a linear function of the attack vector α . Since η_{ϕ} depends on both the attack vector α and the communication result vector ϕ , all possible combinations of BDD results must be taken into consideration when solving this problem⁴. For example, in a distribution network with $E+U$ sensors, including PMUs and EV counters, there are 2^{E+U} possible communication results, each resulting in a specific \mathbf{z}^{AR} . As a result, there are $2^{2^{E+U}}$ possible BDD results (i.e., η vectors) because each \mathbf{z}^{AR} either passes BDD or it does not.

Observe that the objective function $\Psi(\alpha)$ of (46) is the weighted sum of several $\psi_{\phi}(\alpha)$ terms, each being similar to the objective function of (18), but for a specific ϕ . Thus,

⁴Each possible combination of BDD results is a unique binary vector $\eta = \{\eta_{\phi}\}_{\forall \phi}$, which results in a different objective function.

Algorithm 1: FDIA Vector Construction

Input: $\mathbf{H}, \mathbf{W}, \mathbf{z}, \mathbf{z}^P, \Omega, \mathcal{V}, \epsilon, \pi(G), \pi(B)$

Output: α^*

```

1  $\alpha_{\eta}^* \leftarrow 0$ ; // Initialization
2 for each vector  $\eta$  do
3   Solve the respective convex QCLP;
4   if Optimal point (denoted  $\alpha'_{\eta}$ ) exists and
      $\Psi(\alpha'_{\eta}) > \Psi(\alpha_{\eta}^*)$  then
5     |  $\alpha_{\eta}^* \leftarrow \alpha'_{\eta}$ ;
6   end
7 end
8 Return  $\alpha_{\eta}^*$ 

```

if the values of $\eta_{\phi}(\alpha)$ elements are fixed, the objective function $\Psi(\alpha)$ becomes a linear function of α and (46f) can be converted to an inequality constraint for each ϕ in the form of $\|\mathbf{r}_{\phi}^A\|_2 \leq \epsilon$. This implies that the feasible set is the intersection of 2^{E+U} ellipsoids which are obtained by squaring the constraints. Hence, for each vector η , the optimization problem is a convex quadratically constrained linear program (QCLP). It can be further shown that this QCLP is a special case of a second order cone program (SOCP) and can therefore be solved efficiently by interior point methods [29].

Algorithm 1 describes how (46) is solved by iterating over the set of η vectors and solving the resulting QCLP in each case. The maximum adverse impact $\Psi(\alpha)$, attained at the solutions of these problems, determines the solution of the original stochastic optimization problem. Note that in Line 4, we check whether the feasible set is empty and discard η if this is the case. This is because an empty feasible set indicates that no attack vector can lead to this specific combination of BDD results under an arbitrary communication result.

IV. CASE STUDIES

To investigate the impact of stochastic communication on the FDIA performance and the vulnerability of the distribution system VR process to this attack, we evaluate the proposed FDIA on the IEEE 33-bus test feeder [30] and a simplified version of the IEEE 123-bus test feeder [31]. Fig. 2 and 3 depict where charging stations and distribution-level PMUs are installed in these systems. To guarantee accurate state estimation, the minimum number of PMUs should be between 1/5 and 1/3 of the total number of buses [32]. Thus, we consider a total of 7 PMUs in IEEE 33-bus test feeder and 10 PMUs in the simplified IEEE 123-bus test feeder. The pseudo measurement of PMUs can be obtained from the historical data if needed. The pseudo measurement of EVCS counters are obtained from the EVCS queuing model presented in Section II-B. Following [33], we set the error of magnitude and phase angle measurements to be an additive white Gaussian noise, $N(0, 0.01)$ and $N(0, 0.005)$, respectively. The base loads and PMU pseudo measurements are generated according to [34], and the pseudo measurement error is assumed to be an additive white Gaussian noise $N(0, 0.09)$ [35].

To simulate the stochastic communication process, we use an open-source co-simulation platform developed in [36]. In this platform, OpenDSS is utilized for power flow analysis

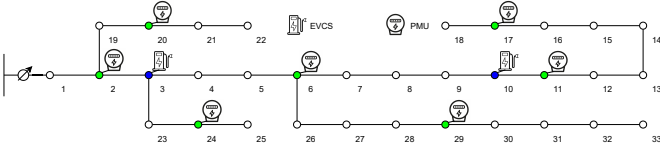


Fig. 2: IEEE 33-bus test feeder topology

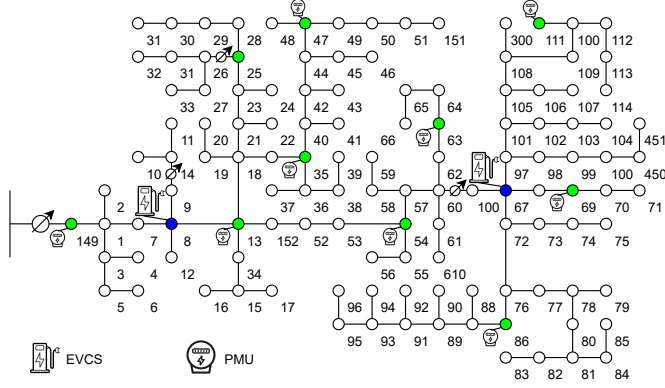


Fig. 3: IEEE 123-bus test feeder topology

TABLE I: Mean Absolute Percentage Error of Δv_ϕ

Circuit	Nonlinear PFA	Linear PFA
IEEE 33-bus test feeder	0.714%	1.654%
IEEE 123-bus test feeder	1.154%	1.916%

(PFA) and a network simulator component is used to capture the communication bit error rate. The bit error rate is set to 0.01, the communication involves small frames with a payload of 32 bits, and framing overhead is considered negligible. The communication network topology is assumed to be a star, with the DSO at the center of the star.

There are 2 charging stations in each distribution system. It is assumed that each EV counter sends the EV count in the respective EVCS to the DSO via the same communication network as PMUs. We use real data to generate the initial SOC, charging demand, and parking time of EVs that visit an EVCS. Specifically, the charging demand is approximated based on the product of trip distance, in the NHTS dataset [37], and the average energy consumption per mile together with the battery size and corresponding maximum driving mileage obtained from [38]. The charging power and parking time are obtained from the EVnetNI dataset [39]. A log-normal distribution with expected value of 0.6848 and standard deviation of 0.9353 is fitted to the empirical distribution of parking times. The charging power is divided into 23 discrete levels from 1 to 23 kW, and the empirical probability mass function is obtained from the dataset. The initial SOC of EVs is generated given the battery size and daily trips. In each EVCS, 50 parking stalls are assumed to be equipped with chargers that support charge powers ranging from 1 to 23 kW.

We study how the proposed FDIA affects the VR process and compare its performance assuming stochastic communication (SC) with the traditional FDIA that builds on an idealized communication (IC) model [11]. Three cases will be mainly discussed: original case without FDIA, FDIA with IC, and FDIA with SC. Before discussing the FDIA performance, we look at the error introduced in the original case in the DSSE

process, which is repeated once every 10 minutes (144 runs in a day), due to linearizing power flow equations (Section II-E). Both the nonlinear PFA and linearized PFA approaches are tested through co-simulation and the mean absolute percentage error (MAPE) of the VR capacity estimation in each case is reported in Table I. It can be readily seen that the approximation done in the linearized PFA does not introduce significant additional error compared to the nonlinear analysis.

We now evaluate the performance of the proposed FDIA with SC in a case study that involves the IEEE 33-bus test feeder, where an FDIA vector is computed in every time slot (10 min) and the total duration of our simulation is one day. Fig. 4 shows the VR estimation error caused by the FDIA vectors bypassing the BDD. We can see that FDIAs can cause a noticeable VR capacity estimation error, i.e., $\psi(\alpha)$. Compared to FDIA with IC, the proposed FDIA (with SC) can effectively mislead the DSO, resulting in similar VR capacity estimation errors with higher BDD pass rate⁵. In particular, the FDIA with SC increases the MAPE of the VR capacity estimation to 427% and the FDIA with IC increases it to 433%, which is slightly higher but results in a much higher detection rate.

In addition to the increased VR capacity estimation error, the negative impact of FDIAs on the voltage profiles is also more pronounced. As shown in Fig. 5, both FDIAs computed by the attacker can result in under-voltage incidents (voltage dropping below $0.95pu$). This is while there is no under-voltage incidents without FDIA because the DSO can accurately estimate the EVCS VR capacity and the insufficient capacity is met by other VR resources. But, the DSO issues an erroneous VR request under FDIA. Since the EVCS VR capacity is overestimated and the actual VR capacity is not enough to satisfy the VR request, serious damages can be inflicted on the power system. Moreover, considering the randomness of the communication process, the proposed FDIA with SC causes 41 under-voltage incidents during one day, which is approximately twice the number of incidents seen in the case of FDIA with IC. This can be attributed to the higher number of modified measurements that manage to go past BDD as can be seen in the bottom subplot of Fig. 5 (the two heatmaps). Recall that not all injected false data can be received by the DSO in time for VR optimization due to the stochastic packet drops that occur in the communication network. Thus, the attack vector that bypasses BDD mechanisms in theory might be actually detected. By considering the packet drop probability, the proposed FDIA can increase the BDD pass rate from around 45% to 99.3% (i.e., one under-voltage incident in 144 time slots); this greatly increases the stealthiness of FDIA. From Fig. 6 we can also conclude that the proposed FDIA is more likely to create under-voltage incidents than FDIA with IC.

Next, we turn our attention to the case study that involves the IEEE 123-bus test feeder. The goal is to show that in a large distribution system, the performance of the proposed FDIA does not fall apart. As it can be seen in Fig. 7, the

⁵There are many more blue markers than red markers which indicate that more attack vectors did not pass BDD in the case of FDIA with IC.

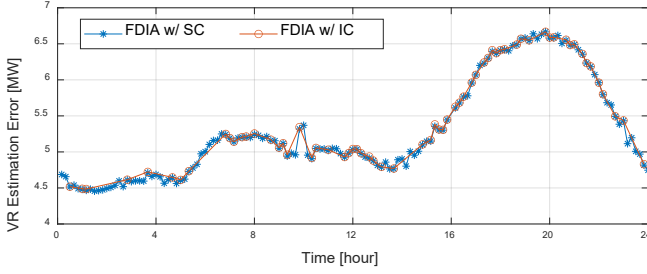


Fig. 4: Comparison of VR capacity estimation error in the IEEE 33-bus system. Note that a dot/marker is drawn only when the attack vector bypasses BDD.

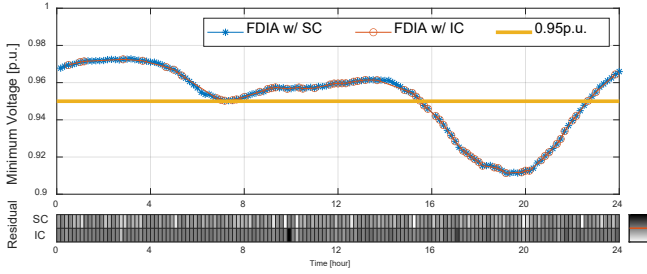


Fig. 5: Comparison of minimum voltage magnitude and BDD pass rate in the IEEE 33-bus system. The heatmaps below this figure show the value of $\|r_\phi^A\|_2^2$ and the horizontal (red) line in the colorbar marks the color intensity of ϵ^2 . Thus, any point that is painted with a lighter gray corresponds to an attack that has bypassed BDD.

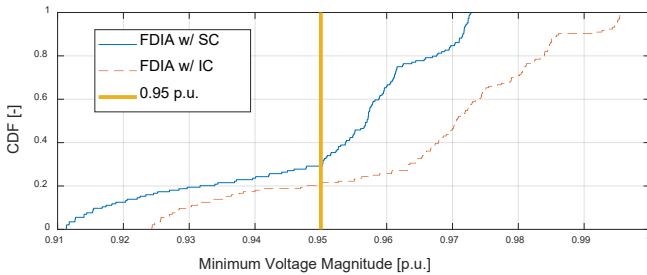


Fig. 6: Cumulative distribution function of the minimum voltage magnitude in the IEEE 33-bus system.

MAPE of VR capacity estimation caused by FDIA with SC is 674%, which is on par with the 691% relative error caused by FDIA with IC. We witness that FDIA with IC introduces a higher error than FDIA with SC (especially from 16:00 to 22:00), but this comes at the cost of being detected. As shown in Fig. 8, the FDIA with IC causes 26 under-voltage incidents, while the proposed FDIA causes 47 incidents. By inspecting the BDD pass ratio and the corresponding under-voltage incidents, it is evident that the attacker can also achieve a better performance when it considers the stochasticity of data communication. The greater potential of the proposed FDIA to cause more detrimental under-voltage incidents in larger distribution systems is depicted in Fig. 9.

V. CONCLUSION AND FUTURE WORK

This paper proposes a novel FDIA against EVCS-mediated voltage regulation which has been the subject of several studies recently. This attack considers potential delays and packet losses in the communication network and the stochastic mobility pattern and charging demand of an EV fleet to maximize its expected adverse impact on the distribution system over time. We carry out simulation on two standard test feeders using a co-simulation platform to showcase the greater potential of

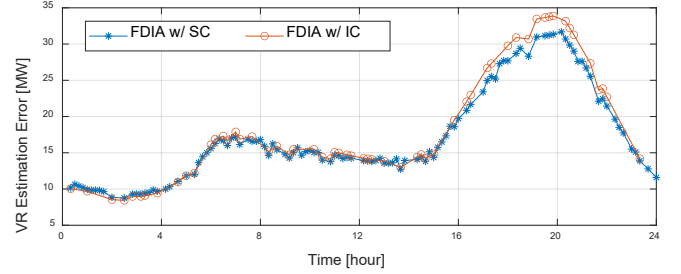


Fig. 7: Comparison of VR capacity estimation error in the IEEE 123-bus system. Note that a dot/marker is drawn only when the attack vector bypasses BDD.

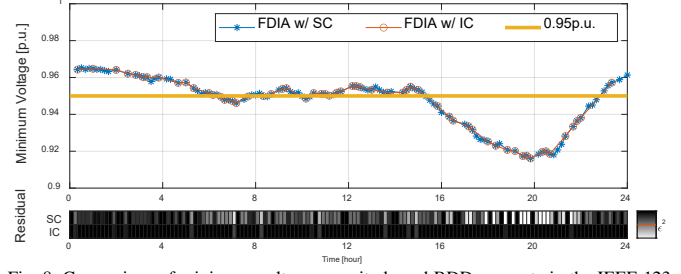


Fig. 8: Comparison of minimum voltage magnitude and BDD pass rate in the IEEE 123-bus system. The heatmaps below this figure show the value of $\|r_\phi^A\|_2^2$ and the horizontal (red) line in the colorbar marks the color intensity of ϵ^2 . Thus, any point that is painted with a lighter gray corresponds to an attack that has bypassed BDD.

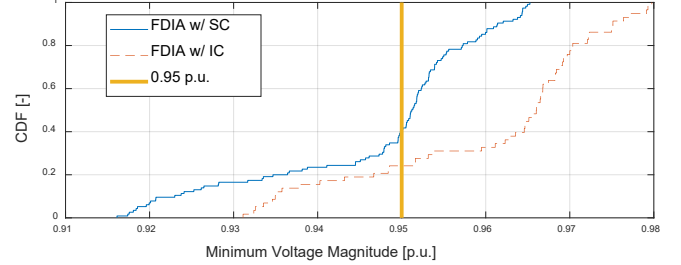


Fig. 9: Cumulative distribution function of the minimum voltage magnitude in the IEEE 123-bus system.

this FDIA to inflict damage compared to the state-of-the-art FDIA attack that relies on an idealized communication model. Our result highlights the vulnerability of the existing BDD mechanism that protects the DSSE process.

In future work, we intend to extend the BDD mechanism to address this vulnerability. A possible approach to detect such an attack is for the DSO to consider various communication results in a network simulator to decide if the received measurement can be trusted. This can help to improve the detect rate and complicate the attack vector construction process, thereby preventing the attacker from solving it in a timely fashion. Furthermore, we plan to develop a probabilistic model for the participation of EVs as economic resources in the VR process. This model will capture the battery degradation cost and incorporate the monetary incentive that will be provided to individual EVs.

REFERENCES

- [1] K. Reddy and S. Meikandasivam, "Load flattening and voltage regulation using plug-in electric vehicle's storage capacity with vehicle prioritization using ANFIS," *IEEE Trans. Sustain. Energy*, vol. 11, no. 1, pp. 260-270, Jan. 2020.
- [2] S. Amamra and J. Marco, "Vehicle-to-grid aggregator to support power grid and reduce electric vehicle charging cost," *IEEE Access*, vol. 7, pp. 178528 – 178538, Dec. 2019.

- [3] L. Cheng, Y. Chang, and R. Huang, "Mitigating voltage problem in distribution system with distributed solar generation using electric vehicles," *IEEE Trans. Sustain. Energy*, vol. 6, no. 4, pp. 1475-1484, Jul. 2015.
- [4] "Literature review on false data injection attack against power system," in *Prof. IEEE SoutheastCon'20*, pp. 1-5, Mar. 2020.
- [5] X. Cai et al., "Review of cyber-attacks and defense research on cyber physical power systems," in *Proc. IEEE iSPEC'19*, pp. 487-492, Nov. 2019.
- [6] Y. Liu, P. Ning, and M. Reiter, "False data injection attacks against state estimation in electric power grids," *ACM Trans. Inf. Syst. Secur.*, vol. 14, no. 1, pp. 21-32, Jun. 2011.
- [7] G. Liang et al., "The 2015 Ukraine blackout: implications for false data injection attacks," *IEEE Trans. Power Syst.*, vol. 32, no. 4, pp. 3317-3318, Jul. 2017.
- [8] M. Esmalifalak et al., "Detecting stealthy false data injection using machine learning in smart grid," *IEEE Syst. J.*, vol. 11, no. 3, pp. 1644-1652, Sep. 2017.
- [9] S. Wang, S. Bi, and Y.-J.-A. Zhang, "Locational detection of the false data injection attack in a smart grid: A multilabel classification approach," *IEEE Internet Things J.*, vol. 7, no. 9, pp. 8218-8227, Sep. 2020.
- [10] Y. He, G. J. Mendis, and J. Wei, "Real-time detection of false data injection attacks in smart grid: A deep learning-based intelligent mechanism," *IEEE Trans. Smart Grid*, vol. 8, no. 5, pp. 2505-2516, Sep. 2017.
- [11] D. Choeum and D. Choi, "OLTC-induced false data injection attack on Volt/VAR optimization in distribution systems," *IEEE Access*, vol. 7, pp. 34508-34520, Mar. 2019.
- [12] A. Sayghe et al., "Survey of machine learning methods for detecting false data injection attacks in power systems," *IET Smart Grid*, vol. 3, no. 5, pp. 581-595, Oct. 2020.
- [13] M. Rana, R. Bo, and A. Abdelhadi, "Distribution grid state estimation under cyber attacks using optimal filter and bayesian approach," *IEEE Syst. J.*, vol. 15, no. 2, pp. 1970-1978, Aug. 2020.
- [14] D. Xue, X. Jing, and H. Liu, "Detection of false data injection attacks in smart grid utilizing ELM-Based OCON framework," *IEEE Access*, vol. 7, pp. 31762-31773, Apr. 2019.
- [15] N. Bhusal, M. Gautam, and M. Benidris, "Detection of cyber attacks on voltage regulation in distribution systems using machine learning," *IEEE Access*, vol. 9, pp. 40402-40416, Mar. 2021.
- [16] Y. Iozaki et al., "Detection of cyber attacks against voltage control in distribution power grids with PVs," *IEEE Trans. Smart Grid*, vol. 7, no. 4, pp. 1824-1835, Jul. 2016.
- [17] P. Zhuang and H. Liang, "False data injection attacks against state-of-charge estimation of battery energy storage systems in smart distribution networks," *IEEE Trans. Smart Grid*, vol. 12, no. 3, pp. 2566-2577, May. 2021.
- [18] R. Kaviani and K. Hedman, "A detection mechanism against load-redistribution attacks in smart grid," *IEEE Trans. Smart Grid*, vol. 12, no. 1, pp. 704-714, Jan. 2021.
- [19] S. Sahoo et al., "A stealthy cyber-attack detection strategy for DC Microgrids," *IEEE Trans. on Power Electron.*, vol. 34, no. 8,
- [20] S. Basumallik, S. Eftekharijad, and B. K. Johnson, "The impact of false data injection attacks against remedial action schemes," *Int. J. Electr. Power Energy Syst.*, vol. 123, Dec. 2020.
- [21] A. Abbaspour et al., "Resilient control design for load frequency control system under false data injection attacks," *IEEE Trans. Ind. Electron.*, vol. 67, no. 9, pp. 7951-7962, Sep. 2020.
- [22] K. Mehmood et al., "A real-time optimal coordination scheme for the voltage regulation of a distribution network including an OLTC, capacitor banks, and multiple distributed energy resources," *Int. J. Electr. Power Energy Syst.*, vol. 94, pp. 1-14, Jan. 2018.
- [23] K. Reddy and S. Meikandasivam, "Load flattening and voltage regulation using plug-in electric vehicle's storage capacity with vehicle prioritization using ANFIS," *IEEE Trans. Sustain. Energy*, vol. 11, no. 1, pp. 260-270, Jan. 2020.
- [24] D. Ding et al., "Recursive secure filtering over Gilbert-Elliott channels in sensor networks: the distributed case," *IEEE Trans. Signal Inf. Proc. Netw.*, vol. 7, pp. 75-86, Dec. 2020.
- [25] P. Zhuang, R. Deng, and H. Liang, "False data injection attacks against state estimation in multiphase and unbalanced smart distribution systems," *IEEE Trans. Smart Grid*, vol. 10, no. 6, pp. 6000-6013, Nov. 2019.
- [26] C. Liu et al., "Joint admittance perturbation and meter protection for mitigating stealthy FDI attacks against power system state estimation," *IEEE Trans. Power Syst.*, vol. 35, no. 2, pp. 1468-1478, Mar. 2020.
- [27] H. Yuan et al., "Novel linearized power flow and linearized OPF models for active distribution networks with application in distribution LMP," *IEEE Trans. Smart Grid*, vol. 9, no. 1, pp. 438-448, Jan. 2018.
- [28] R. Swendsen, *An introduction to statistical mechanics and thermodynamics*. USA, Oxford University Press, 2020.
- [29] S. Boyd and S. P. Boyd, "Convex optimization," Cambridge University, Mar. 2004.
- [30] M. E. Baran and F. F. Wu, "Network reconfiguration in distribution systems for loss reduction and load balancing," *IEEE Tran. Power Deliv.*, vol. 4, no. 2, pp. 1401-1407, Apr. 1989.
- [31] S. Bolognani and S. Zampieri, "On the existence and linear approximation of the power flow solution in power distribution networks," *IEEE Trans. Power Syst.*, vol. 31, no. 1, pp. 163-172, Jan. 2016.
- [32] T. Baldwin et al., "Power system observability with minimal phasor measurement placement," *IEEE Trans. Power Syst.*, vol. 8, no. 2, pp. 707-715, May 1993.
- [33] P. Zhuang and H. Liang, "False data injection attacks against state of charge estimation of battery energy storage systems in smart distribution networks," *IEEE Trans. Smart Grid*, vol. 13, no. 3, pp. 2566-2577, May. 2021.
- [34] E. Wilson, "Commercial and residential hourly load profiles for all TMY3 locations in the United States," National Renewable Energy Laboratory, Nov. 2014. [Online]. Available: <https://data.openepi.org/submissions/153>.
- [35] R. Singh, B. Pal, and R. Vinter, "Measurement placement in distribution system state estimation," *IEEE Trans. Power Syst.*, vol. 24, no. 2, pp. 668-675, May 2009.
- [36] E. Souza, O. Ardakanian, and I. Nikolaidis, "A co-simulation platform for evaluating cyber security and control applications in the smart grid," in *Proc. IEEE ICC'20*, pp. 1-7, Jul. 2020.
- [37] Federal Highway Administration. (2017). 2017 National Household Travel Survey, U.S. Department of Transportation, Washington, DC. Available online: <https://nhts.orl.gov>.
- [38] "Useable battery capacity of full electric vehicles," *Electric Vehicle Database*. [Online] Available: <https://ev-database.org/cheatsheet/useable-battery-capacity-electric-car>.
- [39] "ElaadNL open EV charging transactions," Jan. 2020. [Online]. Available: <https://platform.elaad.io/download-data/>.